Article

Influence of Hydrogen Ions on the Performance of Thin-Film Transistors with Solution-Processed AlO$_x$ Gate Dielectrics

Yongbo Wu, Linfeng Lan *[ID], Penghui He, Yilong Lin, Caihao Deng, Siting Chen and Junbiao Peng

State Key Laboratory of Luminescent Materials and Devices, South China University of Technology, Guangzhou 510640, China; mswuyongbo@mail.scut.edu.cn (Y.W.); 201610102263@mail.scut.edu.cn (P.H.); 201820109593@mail.scut.edu.cn (Y.L.); msdengcaihao@mail.scut.edu.cn (C.D.); mschensiting@mail.scut.edu.cn (S.C.); psjbpeng@scut.edu.cn (J.P.)
* Correspondence: lanlinfeng@scut.edu.cn

Abstract: Over the past decade, there have been many reports on solution-processed oxide thin-film transistors (TFTs) with high mobility (even >100 cm^2 V^{-1}s^{-1}). However, the capacitance uncertainty of the solution-processed oxide gate dielectrics leads to serious overestimation of the mobility. Here, solution-processed AlO$_x$ dielectrics are investigated systematically, and the effect of mobile ions on the frequency-dependent capacitance of the solution-processed AlO$_x$ dielectrics is also studied. It was found that the capacitance of the AlO$_x$ depends on the frequency seriously when the annealing temperature is lower than 300 °C, and the water treatment causes more seriously frequency-dependent capacitance. The strong frequency-dependent capacitance of the AlO$_x$ annealed at 250 or 300 °C is attributed to relaxation polarization of the weakly bound ions in the incompletely decomposed AlO$_x$ films. The water treatment introduces a large number of protons (H$^+$) that would migrate to the ITO/AlO$_x$ interface under a certain electric field and form an electric double layer (EDL) that has ultrahigh capacitance at low frequency.

Keywords: Aluminum oxide; dielectric; thin-film transistor; solution-processed; oxide semiconductor

1. Introduction

In the past decade, oxide thin-film transistors (TFTs) have drawn much attention for their potential applications in large-size, high-frequency, transparent, flexible, or energy-saving displays due to the advantages of ultralow off-current, relatively high field-effect mobility, good uniformity in large size, etc. [1,2]. In oxide TFTs, the gate dielectric layer plays an important role; therefore, it is necessary to investigate the influence the of gate dielectric materials and their fabrication process on the performance of the oxide TFTs. A number of gate dielectrics such as HfO$_2$ [3,4], Al$_2$O$_3$ [5–10], and ZrO$_2$ [11–15], and giant dielectric constant materials [16] have been investigated for oxide TFTs. However, the effect of the water-induced mobile ions of the gate dielectrics on the TFT performance has not been studied in detailed yet.

Compared to the traditional vacuum-processed method, the solution-processed method is more attractive for the advantages of low-cost, high-throughput, and easy chemical composition control [17]. Recently, solution-processed AlO$_x$ gate dielectric has drawn attention due to the high dielectric constant, low leakage current, and good compatibility with oxide semiconductors [7,18,19]. However, the capacitance of solution-processed AlO$_x$ dielectrics depends on the preparing processes strongly [20,21]. Therefore, it is necessary to investigate the mobile ions and residue groups in the solution-processed AlO$_x$ dielectrics to improve the insulating properties. In addition, there have been many reports on solution-processed oxide TFTs with high field-effect mobility (even >100 cm^2 V^{-1}s^{-1}). These values are highly controversial, because the capacitance used to calculate the field-effect mobility is 1kHz or above, which is much lower than the actual capacitance during TFT measuring (the gate

sweeps at a certain V_{GS} step, which means that the charging of the gate dielectric is step-by-step, meaning quasistatic capacitance is more appropriate for the mobility calculation). For this reason, it is indispensable to regulate the capacitance measurement for calculating the field-effect mobility of TFTs. In this paper, the properties of solution-processed AlO_x dielectrics are investigated systematically, and the effect of mobile protons on the frequency-dependent capacitance and on the performance of the oxide TFTs is also studied.

2. Experiment

The AlO_x precursor solution was prepared by dissolving 0.2 M $Al(NO_3)_3 \cdot 9H_2O$ in 2-methoxyethanol, stirred at room temperature for 24 h, and aged for 6 h. The precursor materials, including solutes and solvents, were purchased from Aladdin. The AlO_x precursor films were deposited by spin-coating at 3000 rpm for 30 s and then soft-baked on a hot plate at 150 °C for 10 min to remove the solvents. After that, the AlO_x precursor films were annealed in the air at different temperature of 250, 300, and 350 °C for 1 h. Each sample was baked at 150 °C for 10 min immediately after spin-coating. Then, each sample was annealed separately at different temperature for 1 h. The thickness of AlO_x is about 57 ± 3 nm.

TFTs with AlO_x gate dielectric layer and $InScO_x$ (In_2O_3:Sc_2O_3 = 98:2 wt%) semiconductor layer were constructed with a bottom-gate top-contact structure. A 200 nm indium tin oxide (ITO, In:Sn = 9:1) gate electrode was deposited onto the glass substrate by DC magnetron sputtering (70 W) under argon pressure of 0.5 Pa at room temperature through a shading mask. Then, a layer of AlO_x dielectric film was deposited onto the ITO gate electrode using the process described above. After that, the $InScO_x$ semiconductor layer (20 nm) was deposited by RF magnetron sputtering (60 W) under argon pressure of 0.5 Pa at room temperature through a shading mask. The ITO source and drain electrodes (200 nm) were deposited onto the $InScO_x$ semiconductor layer by DC magnetron sputtering with the same conditions as that of the gate deposition. The channel width (W) and length (L) were defined by a shading mask to be 800 and 200 μm, respectively. Finally, the TFT devices were post-annealed at 250 °C for 1 h. The ITO/AlO_x/ITO metal-insulator-metal (MIM) devices were prepared by depositing a circular ITO top electrode (200 nm) with a diameter of 0.04 mm onto the AlO_x film by DC magnetron sputtering.

To investigate the effect of hydrogen ions (H^+) on the dielectric properties of the AlO_x layer, water treatment was performed on the surface of the ITO gate electrode before spin-coating the AlO_x film. Because the solution-processed AlO_x film is very sensitive to moisture, water treatment is a simple way to increase the density of the mobile H^+. The water treatment process was performed by spin-coating deionized water at a speed of 3000 rpm for 30 s onto the surface of the ITO gate electrode to introduce large amount of adsorbed H^+ and OH^- groups at the ITO/AlO_x interface. The ITO surface is treated by O_2 plasma before water treatment. The contact angles of the plasma treated and plasma + water treated ITO surfaces are 5.03° and 3.93°, respectively.

The thermal behavior of AlO_x precursor was analyzed by thermogravimetric analyses (TG). The chemical composition, water adsorption, and proton quantity behavior of the AlO_x films were characterized by X-ray photoelectron spectroscopy (XPS, Thermo Fisher Scientific Inc, ESCALAB250Xi), infrared spectroscopy (FT-IR), and time-of-flight secondary-ion mass spectrometry (TOF-SIMS), respectively. The electrical properties of MIM and TFTs were characterized by semiconductor parameter analyzer (Keysight B1500A).

3. Results and Discussion

Figure 1a shows the TG curve of AlO_x precursor. It reveals an initial mass loss event of ~60%, occurring around 120–180 °C, which is assigned to the removal of solvent and organic residues and the dehydroxylation of AlO_x precursor. Then, a slow mass loss is observed around 180–350 °C, with weight stabilizing at close to 20% by 350 °C, indicating complete conversion of precursors to form the dense metal oxide. Figure 1b shows the FT-IR spectra of AlO_x films annealed at different temperatures. The peaks around 1700 cm^{-1} (C=C stretching) and 1500 cm^{-1} (N-O asymmetric stretching) are

attributed to the residual organic elements and the undecomposed precursor metal salts, respectively [22,23]. As the annealing temperature increases from 250 to 350 °C, the intensity of the peaks decreases continuously, which is consistent with the TG analysis. The peaks in the range of 3500–3800 cm^{-1} is due to the peaks of O-H stretching plausibly resulting from surface hydroxylation [22,23].
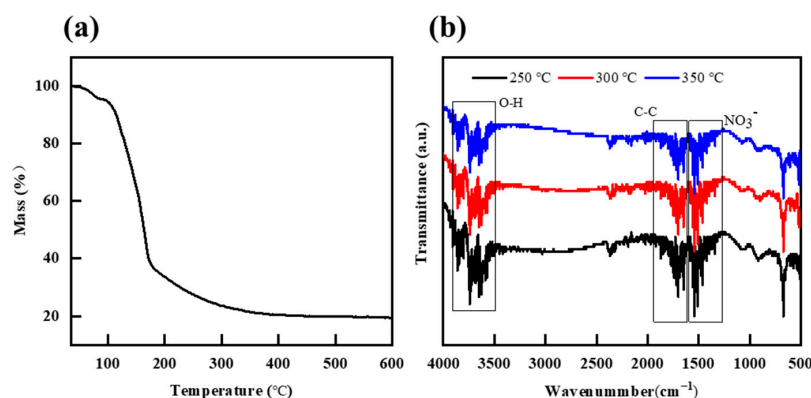

Figure 1. (**a**) TG curve of the AlO$_x$ precursor from 35 to 600 °C. (**b**) FT-IR spectra of the AlO$_x$ films annealed at different temperatures.

Figure 2 shows the XPS O 1s peaks of the AlO$_x$ films with different annealing temperature. Each O 1s spectrum was fitted by two Gaussian distributions with binding energies at 531 and 532.3 eV, corresponding to the contribution of lattice oxygen (M–O–M), and hydroxyl group (M–OH), respectively [7,10,18,21,22]. The relative concentrations of M–OH related oxygen for the untreated samples annealed at 250, 300, and 350 °C are 41.88%, 36.81%, and 25.40%, respectively, while the water-treated samples annealed at 250, 300, and 350 °C exhibit higher M–OH concentrations of 43.06%, 37.60 %, and 25.97%, respectively. The result is in accordance with the change of O-H stretching peaks in the FT-IR spectra (Figure 1b). It indicates that there are plenty of hydroxyl groups on the surface of AlO$_x$ film annealed at 250 °C, and the number of them can be reduced effectively when the annealing temperature reaches 350 °C. The concentration difference between the water-treated and untreated samples narrows as the annealing temperature increases, because the water molecules are easier to be dislodged at higher annealing temperature.
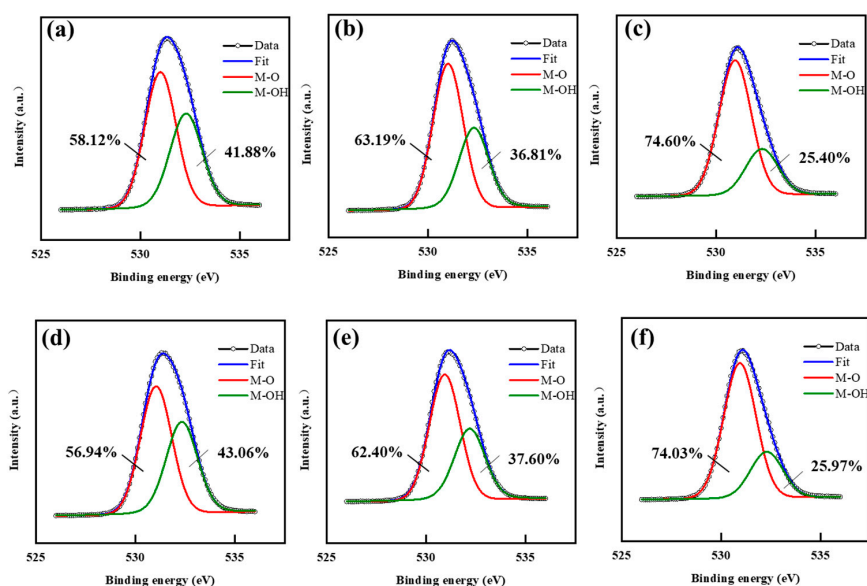

Figure 2. XPS O1s spectra of the untreated AlO$_x$ films annealed at (**a**) 250, (**b**) 300, and (**c**) 350 °C; and XPS O1s spectra of the water treated AlO$_x$ films annealed at (**d**) 250, (**e**) 300, and (**f**) 350 °C.

The insulating properties of AlO_x films were evaluated with a MIM structure of $ITO/AlO_x/ITO$. Figure 3a shows the frequency dependence of capacitance of the MIM devices. Interestingly, the capacitance decreases as the annealing temperature increases at lower frequency regime (<10 kHz), while it increases as the annealing temperature increases at higher frequency regime (>1 MHz). In addition, the capacitance of the MIM devices annealed at 250 or 300 °C depends on the frequency greatly, while the AlO_x film annealed at 350 °C is almost independent of the measuring frequency (when the measuring frequency is lower than 100 kHz). The areal capacitances at 1 kHz for the MIM devices annealed at 250, 300, and 350 °C are 179.1, 166.3, and 148.1 nF/cm^2, respectively; and the areal quasistatic (QS) capacitances (see Figure 3b) for the devices annealed at 250, 300, and 350 °C are 288.9, 263.4, and 152.8 nF/cm^2, respectively. It shows that the areal quasistatic capacitance of the MIM devices annealed at 250 or 300 °C is much higher than those measured at 1 kHz, while there is no much difference between the areal quasistatic capacitance and the areal capacitance at 1 kHz for the one annealed at 350 °C. The strong frequency-dependent capacitance of the MIM devices annealed at 250 or 300 °C is attributed to relaxation polarization of the weakly bound ions in the incompletely decomposed AlO_x films. Especially, the protons (H^+), which can move in the whole AlO_x film, move to the ITO/AlO_x interface and form an electric double layer (EDL) that has ultrahigh capacitance at very low frequency [24,25].
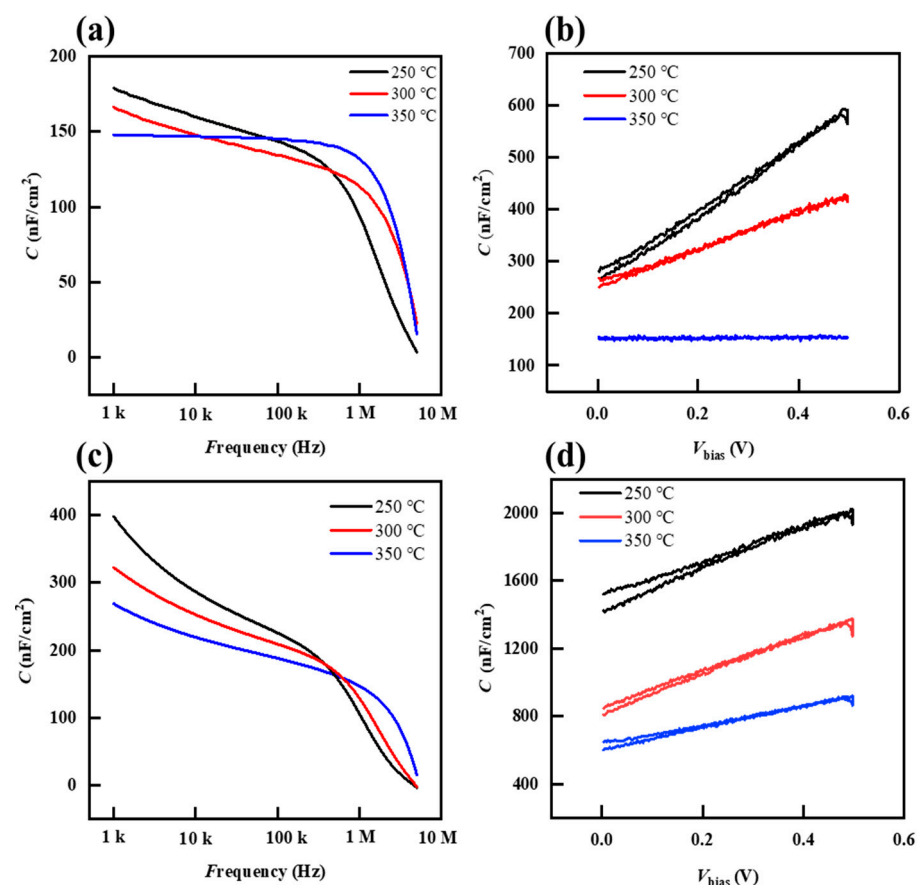

Figure 3. (**a**) Capacitance-frequency curves and (**b**) quasistatic capacitance-voltage curves of the AlO_x dielectrics without water treatment; (**c**) Capacitance-frequency curves; and (**d**) quasistatic capacitance-voltage curves of the AlO_x dielectrics with water treatment.

To further investigate the effect of mobile hydrogen-related ions on the low-frequency capacitance of the AlO_x films, the surface of the bottom electrode (ITO) was treated by water before spin-coating the AlO_x precursor on it. The water treatment can introduce large amounts of the adsorbed water molecules at the ITO/AlO_x interface that would

further form hydrogen and OH groups. Figure 3c shows the frequency dependence of capacitance of the MIM devices with water treatment. It can be seen that the capacitance of all devices (even annealed at 350 °C) depends on the frequency seriously. The areal capacitances at 1 kHz of the MIM devices annealed at 250, 300, and 350 °C are 387.9, 295.3, and 268.9 nF/cm^2, respectively. However, the areal quasi-static capacitances of the MIM devices annealed at 250, 300, and 350 °C are as high as 1520, 846, and 647 nF/cm^2 (see Figure 3d). The extremely high quasistatic capacitance is most probably attributed to H^+ ions which are small and easy to be driven by the electric field. The H^+ ions in oxide films are generally associated with oxygen atoms to form a three-coordinate oxygen center (M–OH+–M), and the motion of H^+ ions is relied on "a sequence of hops" from one bridging oxygen atom to another [13,24,26]. When a voltage is applied to the MIM device, the H^+ ions migrate to the AlO_x/ITO interface by a sequence of hops and form a very thin EDL with an extremely large capacitance. Under an electric field of 0.3 MV/cm (2 V), the leakage current density (*J*) of the MIM devices without water treatment annealed at 250, 300, and 350 °C are 3.2×10^{-8}, 2.4×10^{-8}, and 1.4×10^{-8} A/cm^2, respectively, corresponding to much higher *J* of 5.5×10^{-7}, 4.5×10^{-7}, and 2.6×10^{-7} A/cm^2 for the water-treated ones (not shown). The breakdown field of the MIM devices without water treatment annealed at 250, 300, and 350 °C are 1.9, 2.9, and 3.2 MV/cm, respectively (not shown). Interestingly, the leakage current for the water-treated MIM devices increases greatly at ~0.3 MV, but there are not apparent breakdown points. The difference may be attributed to the large amount of movable H^+ ions in the water-treated AlO_x samples, which form leakage current paths. To verify the existence of H^+ ions in the AlO_x films, TOF-SIMS experiments were carried out. Figure 4 shows the depth-profile element distribution of the water-treated AlO_x/ITO sample annealed at 350 °C. The intensities for the carbon signal are very weak, revealing little carbon-related residuals. By contrast, there are a number of hydrogens in the whole AlO_x dielectric. It is worth noting that the hydrogen distribution is not uniform with the density gradually decreasing from AlO_x surface to the AlO_x/ITO interface. The results confirm that a large amount of hydrogen elements is introduced during treatment. The obvious overlap of Al and In signals is mainly due to the diffusion of Al and In elements at the ITO/AlO_x interface.
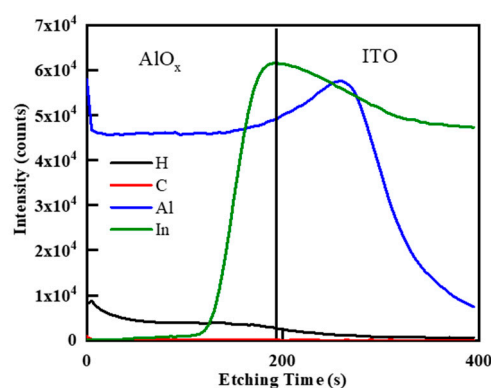

Figure 4. Distribution of H, C, Al, and In elements for the sample of AlO_x film deposited on ITO surface with water treatment and 350 °C annealing analyzed by TOF-SIMS.

Finally, TFTs with AlO_x gate insulator and $InScO_x$ channel layer were fabricated to verify the formation of EDL. $InScO_x$ semiconductor can effectively decrease the influence of water and oxygen in the environment on the stability of TFTs [27]. Figure 5a,b shows the transfer curves of the TFTs without and with water treatment, respectively. Interestingly, the TFT without water treatment exhibits clockwise hysteresis in the transfer curve between forward and reverse gate sweeps, while the one with water treatment exhibits anticlockwise hysteresis. The anticlockwise hysteresis of the water-treated TFT is ascribed to the low migration speed of the H^+ ions [28]. When the gate voltage increases, the H^+ ions migrate to the AlO_x/$InScO_x$ interface slowly; after the gate voltage reaches the highest value

and begin to decrease, some of the H^+ ions still move toward the $AlO_x/InScO_x$ interface, causing further increase in the EDL capacitance. As a result, the current for the reverse sweep is higher than that for the forward sweep (due to the higher capacitance). The saturation mobility (μ_{sat}) was extracted by fitting a straight line to the plot of the square root of the I_D versus V_G and using the following equation:

$$I_D = \frac{W\mu_{sat}C}{2L}(V_G - V_{th})^2 \ldots \tag{1}$$

where C is the areal capacitance of the gate dielectric, and W and L are the channel width and length, respectively. The calculated mobilities for forward- and reversed-sweep curves of the TFTs without water treatment is 6.75 and 9.71 $cm^2\,V^{-1}s^{-1}$, respectively, while those for forward- and reversed-sweep curves of water-treated ones are 6.72 and 5.02 $cm^2\,V^{-1}s^{-1}$, respectively. Although the TFT with water treatment is high on-current, the mobility is lower than that of the TFT without water treatment. The results confirm that the mobility of the water-treated TFTs is overestimated if using the same capacitance (C_i) of the untreated TFTs for calculating mobility. The key properties of the TFTs with/without water treatment are summarized in Table 1.
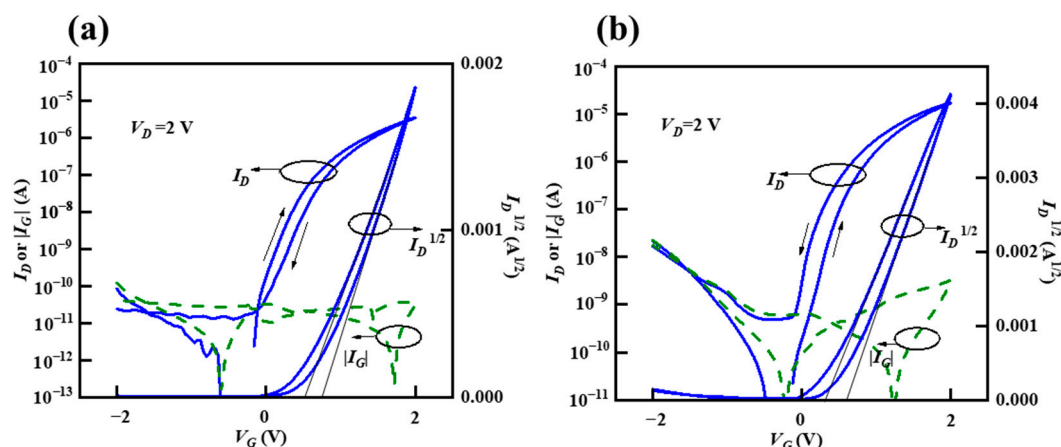

Figure 5. Transfer curves for $InScO_x$ TFTs with AlO_x gate dielectrics (**a**) without and (**b**) with water treatment; the AlO_x gate dielectrics were annealed at 350 °C for 1 h.

Table 1. Electrical properties of the $InScO_x/AlO_x$ TFTs with or without water treatment.

Water Treatment	C/1kHz (nF/cm²)	C/QS (nF/cm²)	V_{th} (V)	μ (cm² V⁻¹s⁻¹)	SS (V dec⁻¹)
With	387.9	647.0	0.61	6.72 (forward) 5.02 (reverse)	0.113
Without	148.1	152.8	0.92	6.75 (forward) 9.71 (reverse)	0.187

4. Conclusions

In summary, MIM and TFT devices based on solution-processed AlO_x dielectrics were fabricated, and the effect of mobile ions on the frequency-dependent capacitance of the solution-processed AlO_x dielectrics is studied. It is found that the capacitance of the AlO_x dielectrics annealed at 250 or 300 °C depends on the frequency greatly, while the AlO_x film annealed at 350 °C is almost independent of the frequency (<100 kHz); and the water treatment causes more seriously frequency-dependent capacitance. The strong frequency-dependent capacitance of the AlO_x annealed at 250 or 300 °C is attributed to relaxation polarization of the weakly bound ions in the incompletely decomposed AlO_x films. The water treatment introduces a large number of protons (H^+) that would migrate

to the ITO/AlO$_x$ interface under a certain electric field and form an electric double layer (EDL) that has ultrahigh capacitance at low frequency. The oxide TFTs based on water treated AlO$_x$ dielectrics exhibit anticlockwise hysteresis in the transfer curves that confirm existence of mobile ions in the AlO$_x$ films. The calculated mobilities for forward- and reversed-sweep curves of the TFTs without water treatment is 6.75 and 9.71 cm^2 V^{-1}s^{-1}, respectively, while those for forward- and reversed-sweep curves of water-treated ones are 6.72 and 5.02 cm^2 V^{-1}s^{-1}, respectively. Although the TFT with water treatment is high on-current, the mobility is lower than that of the TFT without water treatment. The results confirm that the mobility of the water-treated TFTs is overestimated if using the same capacitance (C_i) of the untreated TFTs for calculating mobility.

References

1. Fortunato, E.; Barquinha, P.; Martins, R. Oxide semiconductor thin-film transistors: A review of recent advances. *Adv. Mater.* **2012**, *24*, 2945–2986. [CrossRef]
2. Nomura, K.; Ohta, H.; Takagi, A.; Kamiya, T.; Hirano, M.; Hosono, H. Room-temperature fabrication of transparent flexible thin-film transistors using amorphous oxide semiconductors. *Nature* **2004**, *432*, 488–492. [CrossRef]
3. Cai, W.; Brownless, J.; Zhang, J.; Li, H.; Tillotson, E.; Hopkinson, D.G.; Haigh, S.J.; Song, A. Solution-Processed HfOx for Half-Volt Operation of InGaZnO Thin-Film Transistors. *ACS Appl. Electron. Mater.* **2019**, *1*, 1581–1589. [CrossRef]
4. Jiang, K.; Anderson, J.T.; Hoshino, K.; Li, D.; Wager, J.F.; Keszler, D.A. Low-Energy Path to Dense HfO2Thin Films with Aqueous Precursor. *Chem. Mater.* **2011**, *23*, 945–952. [CrossRef]
5. Daunis, T.B.; Tran, J.M.H.; Hsu, J.W.P. Effects of Environmental Water Absorption by Solution-Deposited Al2O3 Gate Dielectrics on Thin Film Transistor Performance and Mobility. *ACS Appl. Mater. Interfaces* **2018**, *10*, 39435–39440. [CrossRef]
6. Carlos, E.; Dellis, S.; Kalfagiannis, N.; Koutsokeras, L.; Koutsogeorgis, D.C.; Branquinho, R.; Martins, R.; Fortunato, E. Laser induced ultrafast combustion synthesis of solution-based AlOx for thin film transistors. *J. Mater. Chem. C* **2020**, *8*, 6176–6184. [CrossRef]
7. Nayak, P.K.; Hedhili, M.N.; Cha, D.; Alshareef, H.N. High performance In2O3 thin film transistors using chemically derived aluminum oxide dielectric. *Appl. Phys. Lett.* **2013**, *103*. [CrossRef]
8. Park, J.H.; Kim, K.; Yoo, Y.B.; Park, S.Y.; Lim, K.-H.; Lee, K.H.; Baik, H.K.; Kim, Y.S. Water adsorption effects of nitrate ion coordinated Al2O3 dielectric for high performance metal-oxide thin-film transistor. *J. Mater. Chem. C* **2013**, *1*. [CrossRef]
9. Park, K.; Jeon, G.; Lee, S.; Ko, J.; Park, S.-H. Effects of Hydroxyl Group in AlO x Gate Insulator on the Negative Bias Illumination Instability of In-Ga-Zn-O Thin Film Transistors. *Phys. Status Solidi (a)* **2019**, *216*, 1800737. [CrossRef]
10. Xia, W.; Xia, G.; Tu, G.; Dong, X.; Wang, S.; Liu, R. Sol-gel processed high-k aluminum oxide dielectric films for fully solution-processed low-voltage thin-film transistors. *Ceram. Int.* **2018**, *44*, 9125–9131. [CrossRef]
11. Park, J.H.; Yoo, Y.B.; Lee, K.H.; Jang, W.S.; Oh, J.Y.; Chae, S.S.; Baik, H.K. Low-temperature, high-performance solution-processed thin-film transistors with peroxo-zirconium oxide dielectric. *ACS Appl. Mater. Interfaces* **2013**, *5*, 410–417. [CrossRef]
12. Zhu, C.; Liu, A.; Liu, G.; Jiang, G.; Meng, Y.; Fortunato, E.; Martins, R.; Shan, F. Low-temperature, nontoxic water-induced high-k zirconium oxide dielectrics for low-voltage, high-performance oxide thin-film transistors. *J. Mater. Chem. C* **2016**, *4*, 10715–10721. [CrossRef]

13. Li, Y.; Lan, L.; Hu, S.; Gao, P.; Dai, X.; He, P.; Li, X.; Peng, J. Fully Printed Top-Gate Metal–Oxide Thin-Film Transistors Based on Scandium-Zirconium-Oxide Dielectric. *IEEE Trans. Electron. Devices* **2019**, *66*, 445–450. [CrossRef]

14. Lee, C.-G.; Dodabalapur, A. Solution-Processed High-k Dielectric, ZrO2, and Integration in Thin-Film Transistors. *J. Electron. Mater.* **2012**, *41*, 895–898. [CrossRef]

15. Xu, W.; Wang, H.; Ye, L.; Xu, J. The role of solution-processed high-κ gate dielectrics in electrical performance of oxide thin-film transistors. *J. Mater. Chem. C* **2014**, *2*. [CrossRef]

16. Chen, Z.; Lan, L.; Peng, J. Approaching subthreshold-swing limit for thin-film transistors by using a giant-dielectric-constant gate dielectric. *RSC Adv.* **2019**, *9*, 27117–27124. [CrossRef]

17. Chen, R.; Lan, L. Solution-processed metal-oxide thin-film transistors: A review of recent developments. *Nanotechnology* **2019**, *30*, 312001. [CrossRef]

18. Xu, W.; Wang, H.; Xie, F.; Chen, J.; Cao, H.; Xu, J.B. Facile and environmentally friendly solution-processed aluminum oxide dielectric for low-temperature, high-performance oxide thin-film transistors. *ACS Appl. Mater. Interfaces* **2015**, *7*, 5803–5810. [CrossRef]

19. Daunis, T.B.; Barrera, D.; Gutierrez-Heredia, G.; Rodriguez-Lopez, O.; Wang, J.; Voit, W.E.; Hsu, J.W.P. Solution-processed oxide thin film transistors on shape memory polymer enabled by photochemical self-patterning. *J. Mater. Res.* **2018**, *33*, 2454–2462. [CrossRef]

20. Park, H.; Nam, Y.; Jin, J.; Bae, B.-S. Space charge-induced unusually-high mobility of a solution-processed indium oxide thin film transistor with an ethylene glycol incorporated aluminum oxide gate dielectric. *RSC Adv.* **2015**, *5*, 102362–102366. [CrossRef]

21. Jo, J.W.; Kim, J.; Kim, K.T.; Kang, J.G.; Kim, M.G.; Kim, K.H.; Ko, H.; Kim, J.; Kim, Y.H.; Park, S.K. Highly stable and imperceptible electronics utilizing photoactivated heterogeneous sol-gel metal-oxide dielectrics and semiconductors. *Adv. Mater.* **2015**, *27*, 1182–1188. [CrossRef] [PubMed]

22. Xu, W.; Long, M.; Zhang, T.; Liang, L.; Cao, H.; Zhu, D.; Xu, J.-B. Fully solution-processed metal oxide thin-film transistors via a low-temperature aqueous route. *Ceram. Int.* **2017**, *43*, 6130–6137. [CrossRef]

23. Kim, H.; Maeng, S.; Lee, S.; Kim, J. Improved Performance and Operational Stability of Solution-Processed InGaSnO (IGTO) Thin Film Transistors by the Formation of Sn–O Complexes. *ACS Appl. Electron. Mater.* **2021**, *3*, 1199–1210. [CrossRef]

24. Jiang, J.; Wan, Q.; Sun, J.; Lu, A. Ultralow-voltage transparent electric-double-layer thin-film transistors processed at room-temperature. *Appl. Phys. Lett.* **2009**, *95*, 152114. [CrossRef]

25. Mottram, A.D.; Pattanasattayavong, P.; Isakov, I.; Wyatt-Moon, G.; Faber, H.; Lin, Y.-H.; Anthopoulos, T.D. Electron mobility enhancement in solution-processed low-voltage In2O3 transistors via channel interface planarization. *AIP Adv.* **2018**, *8*, 065015. [CrossRef]

26. Norby, T.; Widerøe, M.; Glöckner, R.; Larring, Y. Hydrogen in oxides. *Dalton Trans.* **2004**, 3012–3018. [CrossRef]

27. Song, W.; Lan, L.; Xiao, P.; Lin, Z.; Sun, S.; Li, Y.; Song, E.; Gao, P.; Zhang, P.; Wu, W.; et al. High-Mobility and Good-Stability Thin-Film Transistors With Scandium-Substituted Indium Oxide Semiconductors. *IEEE Trans. Electron. Devices* **2016**, *63*, 4315–4319. [CrossRef]

28. Banger, K.; Warwick, C.; Lang, J.; Broch, K.; Halpert, J.E.; Socratous, J.; Brown, A.; Leedham, T.; Sirringhaus, H. Identification of dipole disorder in low temperature solution processed oxides: Its utility and suppression for transparent high performance solution-processed hybrid electronics. *Chem. Sci.* **2016**, *7*, 6337–6346. [CrossRef]